

# A Methodology for Specifying PET VOI's Using Multimodality Techniques

G. J. Klein,\* *Member, IEEE*, X. Teng, W. J. Jagust, J. L. Eberling, A. Acharya, B. W. Reutter, *Member, IEEE*, and R. H. Huesman, *Member, IEEE*

**Abstract**—Volume-of-interest (VOI) extraction for radionuclide and anatomical measurements requires correct identification and delineation of the anatomical feature being studied. We have developed a toolset for specifying three-dimensional (3-D) VOI's on a multislice positron emission tomography (PET) dataset. The software is particularly suited for specifying cerebral cortex VOI's which represent a particular gyrus or deep brain structure. A registered 3-D magnetic resonance image (MRI) dataset is used to provide high-resolution anatomical information, both as oblique two-dimensional (2-D) sections and as volume renderings of a segmented cortical surface. VOI's are specified indirectly in two dimensions by drawing a stack of 2-D regions on the MRI data. The regions are tiled together to form closed triangular mesh surface models, which are subsequently transformed into the observation space of the PET scanner. Quantification by this method allows calculation of radionuclide activity in the VOI's, as well as their statistical uncertainties and correlations. The methodology for this type of analysis and validation results are presented.

**Index Terms**—Brain, multimodality, positron emission tomography, volume-of-interest.

## I. INTRODUCTION

QUANTITATIVE analysis of multislice positron emission tomography (PET) datasets using regions of interest (ROI's) is a standard technique for studying brain function. A significant aspect of this technique is the process by which one identifies a desired portion of anatomy and then specifies its boundaries as a ROI on a single slice, or a volume of interest (VOI) on a stack of slices. In particular, the availability of multislice scanners with true three-dimensional (3-D) imaging capabilities poses new challenges for 3-D data analysis. Numerous issues related to this process exist which could skew quantitative results if not addressed properly. Because PET data represent functional, not necessarily anatomical information, data from a PET scanner are not al-

ways appropriate for specifying regions. Functional boundaries seen on PET may not correlate with anatomical boundaries, hence, relying on these boundaries while specifying ROI's could easily introduce quantification biases. Even where functional boundaries correspond to anatomical boundaries, the resolution obtained from the highest resolution PET scanners is often inadequate to confidently identify desired anatomical boundaries. For these reasons, many researchers have relied upon other modalities, such as magnetic resonance imaging (MRI), to identify anatomy [1]–[3]. However, even with this multimodality approach, the problem is not completely solved. Typical MRI datasets consist of  $256 \times 256 \times 96$  voxels and are usually displayed as  $256 \times 256$  pixel images, one slice at a time. Trying to identify a region of anatomy, for example a particular gyrus in the cortex, from this slice-based data can be quite difficult even for experienced clinicians. Additional information is required to aid the 3-D navigational task and to convey appropriate cues about the 3-D nature of the anatomy.

In this paper, we describe a methodology for specifying meaningful 3-D VOI's on PET datasets. The methodology is particularly suited for calculation of radiotracer activity and statistical uncertainty in cerebral cortex VOI's representing particular gyri or deep brain structures. The approach addresses two problems that have plagued the specification of such regions in the past. First is the proper identification of a desired anatomical object from a functional PET image. Second is the specification of a true 3-D boundary around that object once it is identified using conventional X-Window interfaces. Unique in the approach is the method by which the regions can be used to accurately model statistical uncertainty of quantified activity in a 3-D acquisition environment.

## II. METHODS

The procedure for obtaining quantitative PET VOI values can be summarized as follows. Three-dimensional ROI's are identified and specified using the high-resolution anatomical data from MRI. The MRI data are registered to multislice PET data using a sequence of manual and automated techniques. VOI boundaries are specified on the MRI dataset by drawing two-dimensional (2-D) regions on a set of parallel image planes. The parallel set of planes may be chosen at any oblique slicing orientation through the MRI volume such that cross sections most clearly show features of the desired anatomical object. Two-dimensional regions are specified on these planes by drawing a freehand polygon or by laying out points which are then connected as a continuous cubic spline. Region

Manuscript received January 22, 1996; revised April 9, 1997. This work was supported in part by the Director, Office of Energy Research, Office of Health and Environmental Research, Medical Applications and Biophysical Research Division of the U.S. Department of Energy under Contract DE-AC03-76SF00098 and in part by the U.S. Department of Health and Human Services under Grants HL25840, AG12435, and AG05890. The Associate Editor responsible for coordinating the review of this paper and recommending its publication was D. Townsend. *Asterisk indicates corresponding author.*

\*G. J. Klein is with the Center for Functional Imaging, Lawrence Berkeley National Laboratory, University of California, Berkeley, CA 94720 USA (e-mail: gjklein@lbl.gov).

X. Teng, W. J. Jagust, J. L. Eberling, A. Acharya, B. W. Reutter, and R. H. Huesman are with the Center for Functional Imaging, Lawrence Berkeley National Laboratory, University of California, Berkeley, CA 94720 USA.

Publisher Item Identifier S 0278-0062(97)05638-3.

drawing on this set of planes is facilitated by the display of a “3-D cursor,” which shows the position not only on the current drawing plane, but also on a number of slices orthogonal to the parallel planes, and on one or more volume renderings of a segmented cortical surface. Further feedback is provided by displaying the intersections of selected regions with these orthogonal slices.

Three-dimensional VOI's are formed by tiling each set of parallel 2-D regions into a closed triangular mesh surface model. A  $4 \times 4$  matrix is calculated which describes the transformation in homogeneous coordinates between the registered MRI and PET, as well as between the original and obliquely resliced MRI. This matrix is used to transform the surface model from the resliced MRI coordinate system into the coordinate system of the PET gantry. Once transformed, the VOI surface models may be used to calculate the activity within a 3-D volume within the PET gantry. In our application, the surface models are currently projected onto the originally acquired PET slices, resulting in a series of labeled 2-D regions. Quantification of activity within these 2-D regions and their uncertainty is achieved by projecting the regions into tomographic sinogram (i.e., Radon or projection) space, and then directly evaluating the counts in this space. Because the full region covariance matrix is available after this calculation, the 2-D region values can be added together, giving an activity value and uncertainty for each PET VOI.

Data referenced in this paper were acquired using a CTI/Siemens ECAT EXACT HR PET scanner [4] and a 1-m bore 0.5-T Oxford MRI magnet with a spectrometer built at our laboratory [5]. MRI volumes comprised a 3-D data set of T1-weighted images (voxel size  $1 \times 1 \times 2$  mm, volume size  $256 \times 256 \times 96$  voxels) acquired using a 3-D gradient recalled echo sequence (TE = 14.3 ms, TR = 30.0 ms). PET data were obtained using the 47-slice scanner in 2-D acquisition mode imaging the radiotracer,  $^{18}\text{F}$ -fluorodeoxyglucose (FDG). An angular compression factor of two was used producing  $336 \text{ bin} \times 196 \text{ angle}$  sinograms with 1.65-mm bin width and 3.125-mm slice separation. The data were reconstructed for use in the segmentation and registration process using standard 2-D filtered backprojection techniques (voxel size  $2.4 \times 2.4 \times 3.1$  mm, volume size  $128 \times 128 \times 47$  voxels) and a Hanning filter with 0.4 cycle/pixel cutoff, corresponding to 5.5-mm transaxial resolution in the center. To correct for the effects of attenuation, data using a  $^{68}\text{Ge}$  rod source in a 20-min transmission scan and a 60-min blank scan were combined to produce appropriate correction factors. Rod windowing was used during transmission and blank acquisition. A normalization file was used to correct each emission, transmission, and blank sinogram on a bin-by-bin basis.

#### A. Segmentation/Registration

In order to relate MRI-based regions to PET measurements, it is necessary to spatially register the two datasets. Automated methods for this process exist but most require that the brain be segmented from nonbrain regions in the MRI data [6], [7]. Some have claimed success using completely automated methods to perform this segmentation [8], however, such tech-

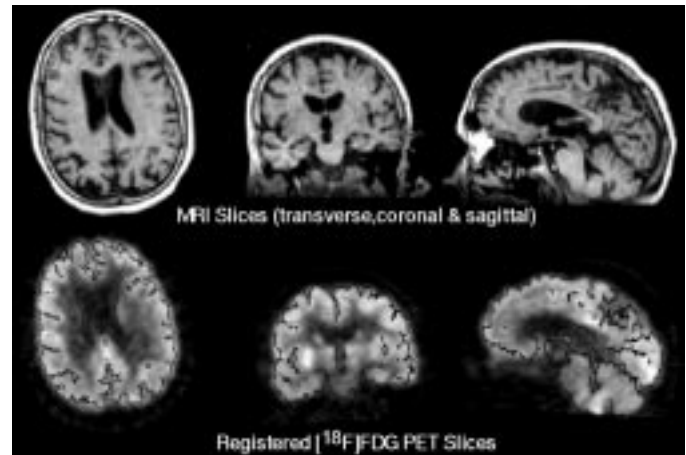


Fig. 1. Manual segmentation. FDG PET data are quickly registered to the MRI dataset using this manual interface. The registered PET data are thresholded and used as a binary mask to automatically segment the brain from nonbrain structures in the MRI. Once the segmentation is obtained, the registration is refined using automated techniques.

niques require special pulse sequences or complex clustering algorithms. In our experiences, finely tuning parameters to obtain a successful segmentation via completely automated results can be quite tedious. We take a simpler approach relying on the facts that in FDG PET images, the outer cortex can be easily segmented from the background using image thresholding, and that the PET and MRI datasets can be approximately registered relatively quickly using manual techniques. As suggested by Pietrzyk [9], the registered and segmented PET data are used to mask the MRI and perform an automatic MRI segmentation. Once the segmented MRI is obtained, it is used to refine the PET registration via automatic techniques. Hence, the bulk of manual interaction that is required for the segmentation and registration exists solely in the “approximate” manual registration step. Note that this technique requires that the brain is entirely within the field of view of the PET scanner.

Fig. 1 shows the interface used to obtain a manual registration. Transverse, sagittal and coronal views of each dataset are simultaneously presented to a user, who is allowed to manipulate translation and rotation parameters. The amount of misregistration can be judged via an interactive cursor showing corresponding points in the six views, or via an edge mask of either dataset which may be overlaid on the other set.

Once an approximate registration is found, the PET data are resliced at the sampling resolution of the MRI volume and are thresholded to form a binary mask. To prevent slight misregistration from masking away brain regions in the MRI, the PET mask is usually dilated using a morphological operator [10]. Further, to prevent masking the inner portions of the MRI brain, the outer boundaries of the PET mask are filled using a 2-D filling operation. The resulting masked MRI dataset is a nearly complete segmentation; however, because the PET mask generally includes some portions of the outer tissue, a 3-D region growing operation seeded from the interior of the cortex is used to obtain the final result. A final step in obtaining an accurate registration is the use of the segmented

MRI dataset in an automated minimum variance of ratios registration technique [7].

After registration and segmentation, an orientation file is stored which describes the registration parameters (six parameters for rigid transformation without scaling). A  $4 \times 4$  transformation matrix can be calculated from this orientation file, and it may be used to relate voxel positions in one volume to their corresponding positions in the resliced registered volume.

### B. Volume of Interest Construction

*Region Drawing Environment:* Rather than attempting to create a sophisticated virtual reality environment for directly sculpting 3-D VOI's, our approach uses conventional 2-D X-Window interfaces which indirectly specify surfaces through a sequence of 2-D operations. That is, VOI's are constructed by drawing stacks of 2-D regions. The region drawing environment makes use of two main principles to carry out this task. First, because the cross-sectional 2-D geometry of an object boundary can usually be simplified just by reslicing along a different orientation, we allow the user to select a set of parallel slicing planes at an angle different from the original acquisition planes. For cortical regions, the typical reslicing orientation is the coronal view of a transversally acquired MRI. However, in general, these reslice orientations can be at any oblique angle with respect to the original acquisition orientation. Second, to aid in the 3-D navigational task, simultaneous views of data are provided in different formats: volume rendered surfaces, orthogonal slices or registered PET slices, on which corresponding points can be visually related.

Fig. 2 shows an example of the region drawing environment. Structured around the VIDA software package [11], a main window [Fig. 2(a)], hereafter called the drawing plane, is provided for the user to draw 2-D regions. Regions may be drawn using freehand polygons, laying out points connected via a cubic spline algorithm, or a number of other techniques. Auxiliary viewing planes sliced at orthogonal angles (e.g., sagittal and transverse when the drawing plane is coronal) can be seen as well. A 3-D cursor, reflecting the position of the drawing cursor, is projected on these views using a parallel projection technique. At any time, a key may be hit while in the drawing plane to update the auxiliary views and display the orthogonal slices intersecting the current main cursor position at that orientation. As a stack of 2-D regions are drawn, their position with respect to one another may be displayed by showing the intersection with the auxiliary orthogonal planes [Fig. 2(b)]. Additionally, to provide guiding points while drawing regions on the drawing plane, curves may be drawn on the auxiliary views and their intersection with the drawing plane will be displayed.

For specifying cortical regions, probably the most useful visual cue is a rendering of the cortical surface. Historically, rendering techniques have been grouped into two subclasses; surface rendering and volume rendering. In surface rendering, a vector model is extracted from the underlying volumetric data and displayed as a set of shaded polygons. This technique has the advantage that it can make use of commonly available

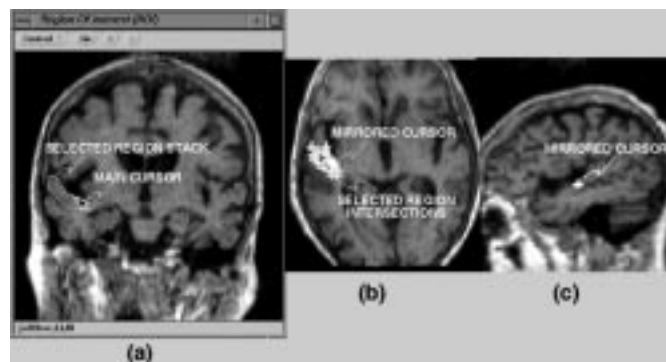


Fig. 2. Region drawing environment. (a) A main drawing window is used to draw 2-D regions. The main window cursor position is mirrored in real-time on auxiliary views (b) and (c) as a projected 3-D cross-hair cursor aids visualization of the 3-D anatomy (cursor size is enlarged here for emphasis). Intersections of selected region stacks with the auxiliary planes (b) give the user intuition of the 3-D shape of the resulting VOI.

graphics hardware for real-time user interaction. It has the disadvantage that the process of extracting the polyhedral model can be extremely computationally intensive, and the model requires considerable storage to adequately describe a surface with enough detail. Volume renderings, on the other hand, are directly calculated from volume data and generally result in a single static image from one perspective of the shaded surface. An advantage is that high-quality volume renderings can be calculated quickly; however, once calculated, little interaction is possible if the depth map is not saved because most of the 3-D information has been lost.

We calculate volume renderings using a parallel projection gradient shaded technique on the segmented MRI data. Because a depth map calculated during the rendering is retained along with the corresponding transformation matrix, the 3-D position of each point in the rendered surface can be calculated. Therefore, visual cues may be provided in two ways. First, a 3-D polyline may be drawn on the rendered brain surface, and its intersections with the 2-D drawing plane will be shown (Fig. 3). This technique is useful for following a specific cortical gyrus through subsequent 2-D slices. A second method provides real-time feedback between the drawing cursor and the volume rendering. As the cursor is moved in the drawing plane, its position in the rendering may be displayed as the projection of the cursor position along the line of sight used to obtain the rendering. Therefore, as the cursor is moved along the outer boundary of the cortex in the drawing plane, its correct position is seen on the volume rendering of the cortical surface, permitting accurate identification of the cortical gyrus.

In practice, our clinicians find that two orthogonal views (sagittal and transverse for a coronal drawing plane) and one or two volume renderings are adequate for localization of cortical anatomy. Also, though the software is capable of defining VOI's drawn on a number of different oblique slicing orientations, a single slicing direction parallel to the coronal plane is usually chosen for most cortical VOI's. A typical set of 2-D contours drawn for a brain dataset is seen in Fig. 4(a). The contours are tiled together using the NUAGES [12] algorithm to produce a triangular mesh surface model [Fig. 4(b)]. The surface model is integrated into an

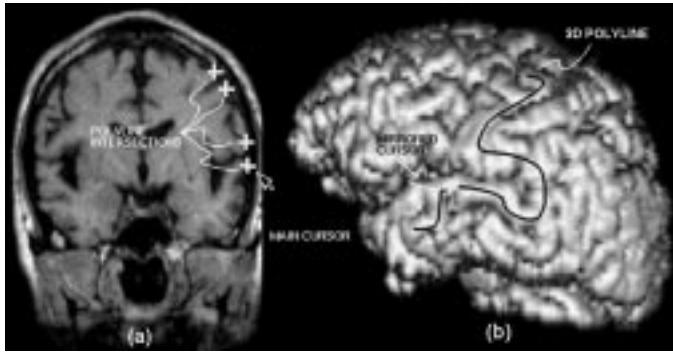


Fig. 3. Volume rendering-based navigation. Three-dimensional positional information is recorded for each pixel in (b) the volume rendering, allowing an interface tying together (a) 2-D sectional with rendered information. Intersections of a polyline drawn on the rendering are shown as crosses on the 2-D view. Position of the cursor in the 2-D view is reflected in the rendering in real time.

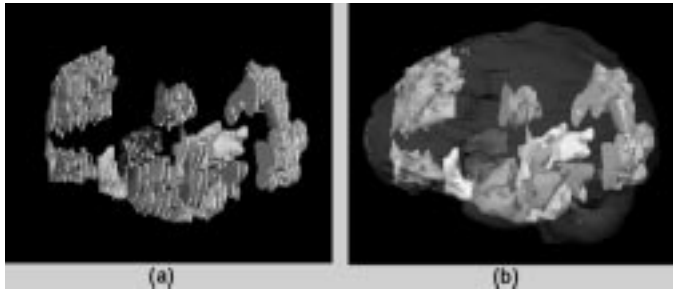


Fig. 4. VOI's. Three-dimensional VOI's are created by tiling stacks of 2-D contours. Contours in (a) are overlaid on the resulting VOI surfaces. A typical set of VOI's drawn for a brain study is seen in (b) in a schematic rendering of the cortical surface.

Inventor toolkit 3-D graphical display environment [13]. In this environment, the user may visualize the resulting 3-D region set and perform a number of arbitrary manipulations on them including scaling, translation and rotation, subdivision, selection, and deletion. VOI's may also be edited by modifying the 2-D contours using spline-based moves, additions or deletions of contour vertices in the 2-D drawing environment.

### C. PET Quantification

*Statistical Quantification:* Quantification of PET activity could take place directly without construction of VOI surface models by reslicing calibrated PET data into the voxel space of the MRI data and summing voxels contained within the boundaries of the 2-D regions. Of course, care must be taken to properly scale calibration factors in accord with the new voxel size of the resliced PET data and to suitably treat voxels on the border of the region. This is the approach, for example, taken by Resnick and coworkers [14]. Besides the possible errors induced from summing edge voxels, there is one main disadvantage to this technique: the uncertainty of the activity data can no longer be accurately characterized; only an approximation is possible [15]. If an accurate estimate of the activity within the region *and* its uncertainty are desired, calculations are easier in the projection, or sinogram space of the tomograph, where the statistical properties are well established [16].

Our approach resembles the formulation of Votaw [17], which generalized Huesman's 2-D ROI algorithm [16]. Define  $E_{lmz}$ ,  $T_{lmz}$ ,  $B_{lmz}$ , and  $N_{lmz}$  as the projection values at bin  $l$ , angle  $m$ , and slice  $z$  for the emission, transmission, blank, and normalization sinograms, respectively. A normalization factor for each slice,  $k_z$ , incorporates correction for deadtime, radiotracer decay, and scan duration and is used to convert reconstructed units into calibrated PET counts/s. Attenuation factors,  $A_{lmz}$ , are calculated as

$$A_{lmz} = \frac{\sum_{m'l'z'} S_{lmz}^{l'm'l'z'} N_{m'l'z'} B_{m'l'z'}}{\sum_{m'l'z'} S_{lmz}^{l'm'l'z'} N_{m'l'z'} T_{m'l'z'}} \quad (1)$$

where  $S_{lmz}^{l'm'l'z'}$  is a 3-D Gaussian smoothing kernel of length 9 and sigma 1.5 bins in all three directions. The corrected projection bin value is then defined by

$$p_{lmz} = E_{lmz} N_{lmz} A_{lmz} k_z. \quad (2)$$

A voxel in the image space of a reconstructed PET volume is given by

$$I_{xyz} = \sum_{km} F_{xy}^{km} \sum_j C_k^j \sum_l R_j^l p_{lmz} \quad (3)$$

where  $F_{xy}^{km}$  are the 2-D backprojection factors,  $I_{xyz}$  is the voxel at location  $(x,y,z)$ ,  $C_k^j$  is the convolutional kernel,  $R_j^l$  are the arc correction rebinning factors, and  $p_{lmz}$  are the projection data. VOI activity in this voxelized space is then given by

$$V_\alpha = \sum_z V_\alpha^z = \sum_z \sum_{x,y \in \alpha_z} I_{xyz} \quad (4)$$

where  $\alpha_z$  denotes the intersection of the VOI indicated by  $\alpha$  and the transverse section indicated by  $z$ . Changing the order of summation and rearranging as in [16] we obtain

$$\begin{aligned} V_\alpha^z &= \sum_{lm} \sum_j R_l^{Tj} \sum_k C_j^k \sum_{x,y \in \alpha_z} F_{xy}^{km} p_{lmz} \\ &= \sum_{lm} h_{\alpha_z}^{lm} p_{lmz} \end{aligned} \quad (5)$$

where

$$h_{\alpha_z}^{lm} = \sum_j R_l^{Tj} \sum_k C_j^k \sum_{x,y \in \alpha_z} F_{xy}^{km}. \quad (6)$$

In going from (3) to (5), we note that though the convolution kernel,  $C_j^k$  is symmetric in  $k$  and  $j$ , the sparse rebinning matrix,  $R_j^l$ , is not symmetric in  $j$  and  $l$  so that its transpose,  $R_l^{Tj}$ , must be used.

To obtain a suitable description of each processed VOI in projection space, that is, a set of sinograms containing the factors  $h_{\alpha_z}^{lm}$ , the VOI is first transformed into the image space of the PET scanner using the  $4 \times 4$  transformation matrix calculated during the PET-MRI registration and during the MRI reslicing processes. The 2-D intersection of the VOI surface model with each acquisition plane is next calculated, resulting in another set of 2-D regions described as closed polygons. Note that at this point the regions are not linked

to the voxel space of a reconstructed PET volume at all, but instead are real-valued  $x, y$  coordinate descriptions in the space of PET scanner. As was suggested by Huesman [16], the forward projection of a given region in this description becomes a continuous integral over the uniformly weighted interior of the polygons

$$\sum_{x, y \in \alpha_z} F_{xy}^{km} \longrightarrow g_{\alpha_z}^{km} = \int_{\alpha_z} F^{km}(x, y) dx dy \quad (7)$$

where  $F^{km}(x, y)$  denotes an indicator function for the ray in projection space at bin  $k$  and angle  $m$ . In practice, this integral can be quickly calculated by taking each polygon line segment in turn and summing the signed area of the trapezoidal region defined by the boundaries of line segment and the projection bins, as seen in Fig. 5(a). Therefore, (6) becomes

$$h_{\alpha_z}^{lm} = \sum_j R_t^{Tj} \sum_k C_j^k g_{\alpha_z}^{km} \quad (8)$$

so that reference to any pixel size is unnecessary. Fig. 5(b) summarizes the overall calculation.

We assume that each individual bin in the sinograms is an independent random variable modeled as a Poisson counting process and make the approximation that the normalization and smoothed attenuation factors are without statistical variation. The emission sinogram values are collected as  $E_{lmz} = E_{lmz}^P - E_{lmz}^R$  where  $E_{lmz}^P$  and  $E_{lmz}^R$  are the emission prompt and random values, respectively. To estimate the number of random coincidences in each projection bin,  $E_{lmz}^R$ , total random events,  $E_z^{RTOT}$  are recorded for each 2-D sinogram so that  $E_{lmz}^R \approx E_z^{RTOT} / LM$ , where  $L$  and  $M$  are the dimensions of the 2-D sinogram. The variance of a single corrected bin is thus,

$$\text{var}(p_{tzm}) = N_{lmz}^2 A_{lmz}^2 k_z^2 \left( E_{lmz} + \frac{2E_z^{RTOT}}{LM} \right) \quad (9)$$

so that for two regions on the same slice, the covariance is given by

$$\text{cov}(V_\alpha^z, V_\beta^z) = \sum_{tm} h_{\alpha_z}^{km} h_{\beta_z}^{km} \text{var}(p_{tzm}). \quad (10)$$

Regions on different slices are uncorrelated so that the covariance for two multislice VOI's is

$$\text{cov}(V_\alpha, V_\beta) = \sum_z \text{cov}(V_\alpha^z, V_\beta^z). \quad (11)$$

Note that in this exposition, we have not yet implemented a correction for scatter. The factory-supplied software for our scanner uses a spatially invariant deconvolution to correct for this effect [4], as suggested by King [18] and Bergstrom [19]. Therefore, this correction can easily be added to the VOI calculation by including an additional convolution operation in (6), which models the scatter distribution.

Calculation of VOI activity by this method has a number of other advantages besides the capability of obtaining statistical properties. Since the high-resolution anatomical data were used to define the VOI boundaries, the PET data do not need to be greatly smoothed to obtain suitable visual image quality. Only a ramp filter is used, preserving spatial resolution

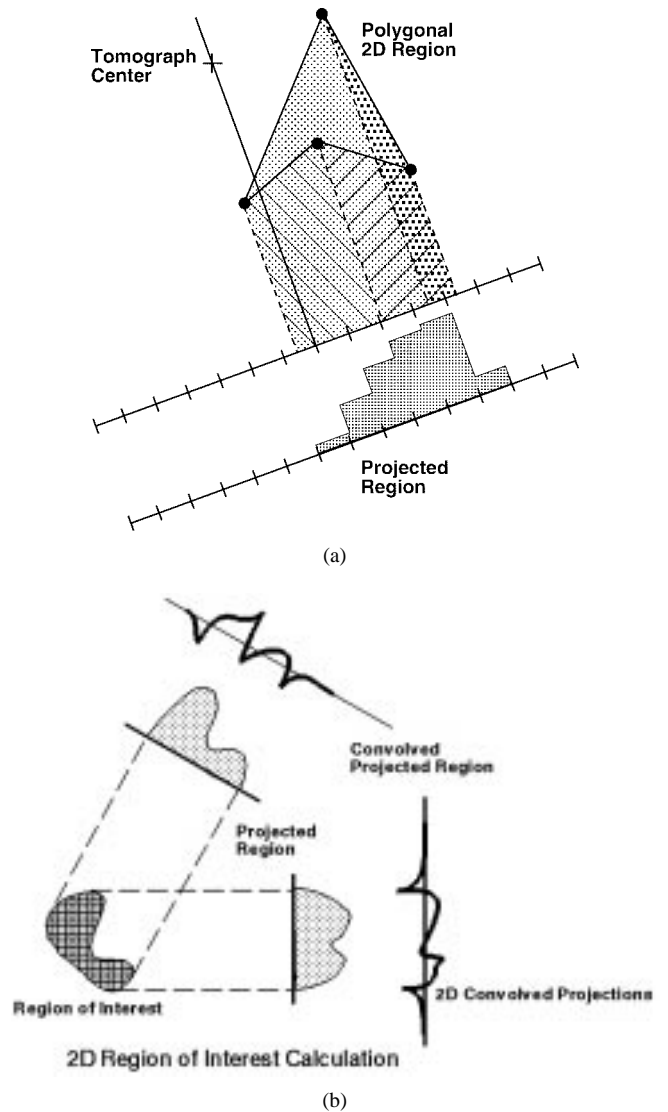


Fig. 5. Projection of a uniform polygonal region. (a) The uniformly weighted interior of a 2-D polygonal region is computed by calculating the signed area of the trapezoids formed by each line segment of the polygon and the projection bins. A simple polygon is shown in this figure to convey the idea. This procedure is carried out for each projection angle, then rebinned and convolved to obtain a sinogram representing the VOI mask in projection space (b). In practice, the 2-D regions are defined by numerous short line segments so that the region boundaries approximate a smooth boundary.

during quantification. Also, because the technique effectively performs a fast reconstruction and summing of the data, reconstruction of a PET image volume is required only to register the data. For dynamic PET acquisitions, it is therefore unnecessary to reconstruct every time point in the data acquisition (although one may wish to do so for other reasons, such as correction for patient motion). Finally, a third advantage is that calculation of VOI values for a 3-D PET acquisition without septa would proceed in a straight-forward manner. In this case, a 2-D forward projection of each VOI would be required at each projection angle, followed by convolution and calculation of the vector inner product. Extending the 2-D projection operation to three dimensions, the signed volume defined by each triangular face and the projection plane can be efficiently computed and binned into the appropriate

locations. Because the geometry of conventional cylindrical scanners prevents complete measurement of sinograms at oblique angles, the 3-D extension of this algorithm differs from the 2-D case in that it requires techniques to properly deal with truncated measured datasets. Defrise *et al.* discuss this in [20]. Computational load and memory requirements grow considerably in the case of 3-D analysis, however, so the overall task of quantifying 3-D data would not be trivial. For example, each VOI mask requires storage space equivalent to a floating point representation of a complete 3-D sinogram (about 300 MB for the ECAT EXACT HR). Obviously, the masks for such a set of VOI's could not reside in the memory of conventional workstations. It is perhaps for this reason that very little has appeared in the literature regarding evaluation of arbitrary VOI's on true 3-D PET datasets. On the other hand, techniques such as additional angular compression, which is routinely used on the ECAT EXACT HR to reduce the 300-MB 3-D dataset to 24 MB, may make this aspect of the problem more manageable.

### III. VALIDATION

While specifying a set of VOI's on a PET dataset, a number of decisions and image processing operations are carried out which could potentially affect the final quantitative results. The accuracy of registration, choice of slice spacing and orientation, and operator criteria for drawing regions are all such factors. Two groups of studies were performed to evaluate the magnitude of quantitative differences due to these factors. The first group used data from a MRI scan obtained from a normal subject. These data were used to evaluate the effects of reslicing the data at different orientations. In the second group, data acquired from two patients were used to evaluate various factors for sets of typical physiologically meaningful VOI's that are drawn manually using the multimodality techniques described in this paper.

#### A. Slicing Orientation

Because the tiling of 2-D contours into a closed triangular mesh surface model is not a well-posed problem with a unique solution, it is important to demonstrate that the direction of slicing and subsequent 2-D region drawing will not dramatically affect the resulting 3-D shape of a VOI. For our application, an important criterion is that the shape of the resulting 2-D intersections of a VOI with the acquisition planes of the PET scanner are consistent regardless of the slicing orientation of the MRI volume used for drawing the VOI. To test this procedure, shape consistency measures were computed for a VOI automatically specified on segmented MRI data resliced at a number of different orientations. We segmented the cortex from the MRI data using techniques described in the paper. These data were then further segmented to produce a  $64 \times 72 \times 12$  voxel rectangular subvolume obtained from the temporal cortex. All nonbrain matter within this subvolume was set to zero. Starting with this dataset as the base volume, the orientation of a reslicing plane was rotated about the  $x$  axis at  $90^\circ$ ,  $60^\circ$ ,  $45^\circ$ ,  $30^\circ$ ,  $0^\circ$ ,  $-30^\circ$ ,  $-45^\circ$ , and  $-60^\circ$  to produce eight  $100 \times 100 \times 70$  voxel derived datasets.

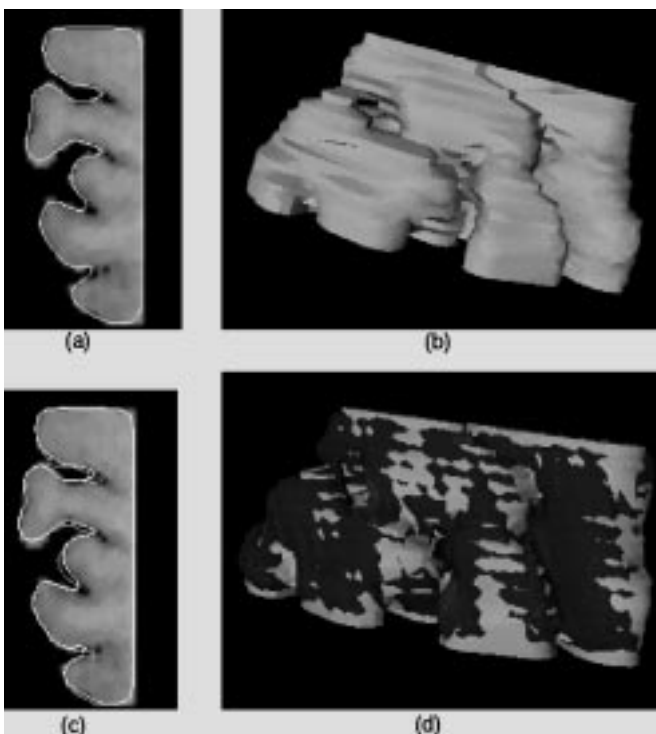


Fig. 6. Reslicing validation study. (a) A slice from the reslicing phantom data set and the contour of an automatically determined 2-D region. (b) Tiling the 2-D region results in a VOI shape typical of ones drawn by clinicians on brain datasets. VOI differences for automatically determined contours from the  $0^\circ$  and  $60^\circ$  slicing orientations displayed via (c) a 2-D slice through the data and (d) overlaid renderings of the VOI's.

Standard trilinear interpolation was used to obtain the resliced volumes. An automatic region-following program was used to obtain a VOI encasing the segmented cortex subvolume in the derived dataset. The automatic technique was used to avoid any operator-induced biases which could occur if manual drawing techniques were used. As seen in a typical slice and volume rendering from the  $0^\circ$  slicing orientation [Fig. 6(a), (b)], the resulting region shape is fairly complex due to the convolutions of the cortex and is representative of typical manually drawn regions.

As is done in the analysis of PET data, a 3-D VOI was constructed from each set of 2-D regions, and then transformed back onto the original  $64 \times 72 \times 12$  voxel subvolume as a new set of 2-D regions. Ideally, each set of transformed 2-D regions should be identical, however, because of tiling and interpolation differences during reslicing, slight variations are seen between the region sets. Fig. 6(c) gives an example of the differences seen between contours on a slice of the  $0^\circ$  slicing orientation versus the  $60^\circ$  slicing orientation, and Fig. 6(d) shows the corresponding VOI renderings for the two slicing orientations.

Three measures were used to characterize the shape difference of the regions. For each measure, the mean difference and standard deviation were calculated for the shape difference measure between the VOI's obtained on the seven resliced datasets and the VOI obtained on the  $0^\circ$  dataset. First, as a simple measure, total volume is computed by summing voxels whose center was contained within the boundaries of

the transformed 2-D regions. Over the eight region sets, the coefficient of variation for VOI volume was 2.3%. However, total enclosed volume gives only a first-order indication of shape consistency. A more meaningful measure of shape difference is the fractional volume difference of each VOI set with respect to a reference, here chosen as the 0° slicing orientation. We define the fractional volume difference as

$$\frac{\text{vol}\{(A \cup B) - (A \cap B)\}}{\text{vol}\{A\}} \quad (12)$$

where  $A$  and  $B$  are two VOI sets,  $\text{vol}\{A\}$  is the volume contained within  $A$ , and  $A$  is the reference VOI.  $\cup$  indicates the union operator and  $\cap$  indicates the intersection operator. More simply, the fractional volume difference is just the total volume which is enclosed by one VOI, but not the other, normalized by the total volume of the reference VOI. The mean fractional volume difference for these regions was  $13.5 \pm 2.9\%$ . Here, and in subsequent portions of this paper, the  $\pm$  term refers to the sample standard deviation of the measures. Another important shape measure giving an indication of the locally worst-case shape difference is the maximum Hausdorff distance [21], defined as

$$\max[d(A, B), d(B, A)] \quad (13)$$

where

$$d(A, B) = \max_{a \in A} \max_{b \in B} |a - b|. \quad (14)$$

The Hausdorff distance, thus, gives the worst-case minimum distance that a point  $a$  in  $A$  is from any point in  $B$ . A related measure, the median Hausdorff distance gives the median minimum distance that all points  $a$  in  $A$  are from any point in  $B$ . Again using the 0° slicing orientation as the reference VOI set, the average maximum Hausdorff distance for these VOI's is  $4.8 \text{ mm} \pm 0.5 \text{ mm}$ , and the average median Hausdorff distance is  $0.54 \text{ mm} \pm 0.02 \text{ mm}$ . In other words, the VOI surface boundaries were mostly within nearly 0.5 mm of each other in these datasets, with occasional outliers up to about 5 mm.

All three shape measures indicate that the area within a desired anatomical region does not depend greatly on the reslicing orientation used to specify the VOI. For the highly convoluted object used in this test, the fractional volume difference was most affected. For objects like these where the surface area to volume ratio is relatively high, small changes in surface boundaries can produce fairly large fractional volume differences. Also note that this measure is particularly sensitive to translation errors, since a small translation error between two identically shaped VOI's results in voxels on both sides of the VOI's in the direction parallel to the translation contributing to the error. A more indicative measure for these data are the Hausdorff measures, which show that there is a small spatial distance between points included in the volume difference and the intersection of the two VOI sets.

## B. PET Quantification Consistency

PET and MRI data from two patients were studied to investigate the consistency of resulting calculated PET VOI activity

with respect to operator region drawing criteria, MRI slice spacing, and MRI-PET registration errors. Six VOI's were drawn in each hemisphere of each patient, using predefined criteria for these regions (dorsolateral frontal cortex, orbital frontal cortex, anterior temporal cortex, posterior temporal cortex, amygdala, and hippocampus). VOI size ranged from a minimum of  $1.1 \text{ cm}^3$  for the amygdala to a maximum of  $13.3 \text{ cm}^3$  for the dorsolateral frontal cortex. Two different operators, each trained in neuroanatomy, drew these regions independently on MRI data which had been resliced into a coronal plane (perpendicular to the line passing through the anterior and posterior commissures) using slices either every 1 mm or every 3 mm. The MRI and PET data were aligned using the technique discussed in Section II-A. VOI's were constructed from each set of 2-D regions and transformed into the PET coordinate space. Subsequently, PET activity for each VOI was calculated in our usual manner by projecting the transformed VOI's into the sinogram space of the PET scanner. Calculated VOI activity concentrations were combined with an arterial input function and known rate constants to obtain regional cerebral metabolic rates for glucose (rCMRglc) via standard methods [22], [23].

Interoperator variance was calculated using the mean difference of ratios over all paired regions drawn by each operator on the 1-mm and 3-mm slices. The difference between operators on the 1-mm slices was  $3.4 \pm 3.0\%$ , with a range between 0.0%–11.0%. The difference between operators on the 3-mm slices was  $4.1 \pm 3.1\%$ , ranging between 0.0%–14.5%. The greatest differences were found to be in the metabolic rates for the hippocampus, presumably because this structure is very difficult to confidently identify even on oblique slices orthogonal to its central axis.

Possible variation due to MRI slice separation was investigated by using the 1-mm separation as a baseline, and subsampling these regions to produce a less dense region set drawn with coronal slice separations of 2, 3, 5, 7, 9, and 11 mm. Percent difference of ratios with respect to the 1-mm baseline from the two operators' regions averaged over all 48 regions (i.e., 12 regions/brain, two brains, two operators) is seen in Fig. 7. As seen from the graph, variation increases slowly as the slice spacing increases (from 0.6% to 2.2%). However, the maximum difference increases quite steeply as the slice separation increases beyond 7 mm.

PET-MRI registration is another factor that can affect quantitative accuracy. Using the coordinates obtained from our registration procedure as a baseline, the mean percent difference of ratios was investigated as translation (along the axes of the MRI coronal volume coordinate system) was added to the transformation matrix. Again, all 48 VOI's drawn on the 1-mm slice separation datasets were used to calculate the statistics. Translation magnitude ranged from 1 mm to 7 mm. Results are presented in Fig. 8(a), (b), (c).

Table I summarizes the overall results. To put these variations in perspective, a baseline region set was drawn to determine statistical variability of PET measurements as they relate to region size. A set of seven square single-slice regions was drawn on six slices in the original transverse PET slices on the two subjects. Region size ranged from  $0.024 \text{ cm}^3$  to

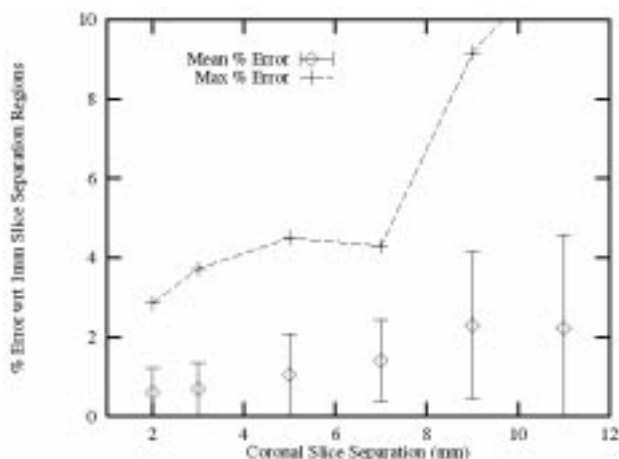


Fig. 7. Quantification consistency—MRI slice spacing. Mean, and maximum difference of ratios in rCMRglc for 24 brain VOI's using the region set drawn on the 1-mm resliced data as a reference. Little difference is seen in this dataset until the MRI slice separation exceeds 7 mm.

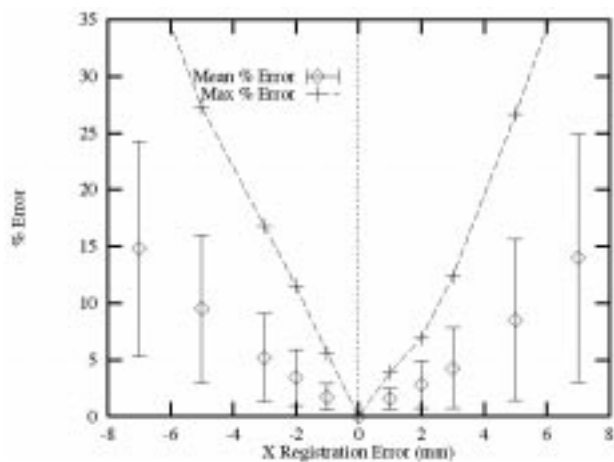
TABLE I  
VOI VALIDATION SUMMARY

	Difference Measure
<b>Reslicing direction</b>	
(volume difference coef. of variation)	2.3%
(fractional difference volume)	13.5 ± 2.9%
(median Hausdorff distance)	0.54 mm ± 0.02 mm
<b>Interoperator</b>	
(mean difference of ratios)	3.4 ± 3.0%
(max difference of ratios)	11.0%
<b>Slice separation: 1–7 mm</b>	
(mean difference of ratios)	0.6 – 1.4%
(max difference of ratios)	2.8 – 4.2%
<b>Slice separation: 9 mm</b>	
(mean difference of ratios)	2.3%
(max difference of ratios)	9.2%
<b>Registration error @ 2 mm</b>	
(mean difference of ratios)	1.9 – 4.1%
(max difference of ratios)	6.6 – 14.1%
<b>Registration error @ 7 mm</b>	
(mean difference of ratios)	5.3 – 14.8%
(max difference of ratios)	14.1 – 141.9%
<b>PET statistical uncertainty</b> (1 cm <sup>3</sup> VOI coef. of variation)	
	1.8%

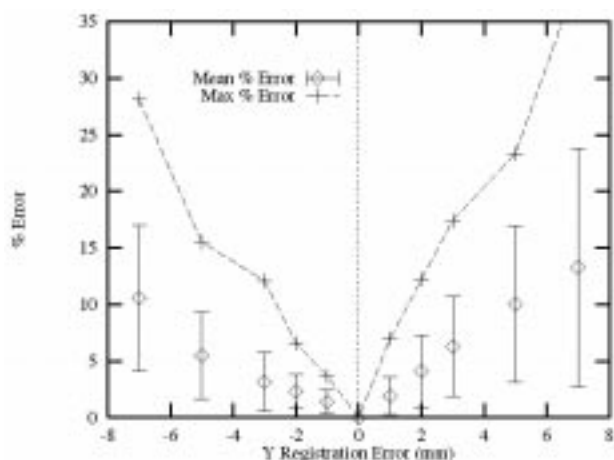
1.03 cm<sup>3</sup>, in other words, from roughly 1 to 57 reconstructed voxels. Using the rCMRglc values and uncertainty calculated for each region, the mean coefficient of variation over the 12 total sets of seven regions was computed. Results are seen in Fig. 9. These values show that uncertainty due to PET statistics decreases as the region size increases. The coefficient for the 1.03-cm<sup>3</sup> region is less than 2%, indicating that for VOI sizes used in the previous results, the uncertainty due to the statistics of the tomograph plays a small role in the overall uncertainty. Of course, these values are subject to the total isotope injected, tomograph sensitivity and scanning time, as well as other factors affecting overall the signal-to-noise ratio of the resulting PET images.

#### IV. DISCUSSION

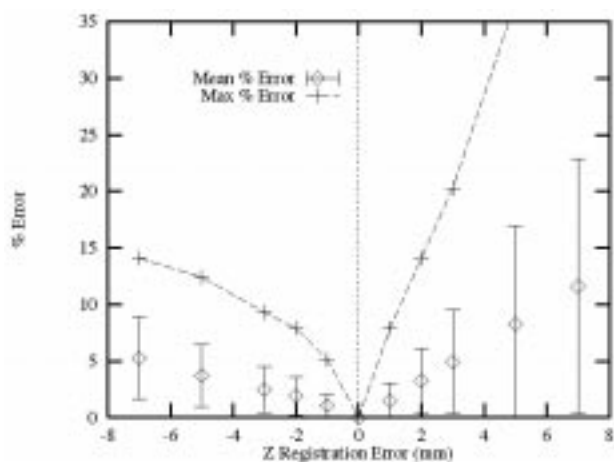
This paper has described several related aspects of PET VOI quantification. We have described an approach which allows



(a)



(b)



(c)

Fig. 8. Misregistration effects on quantification. Translation errors between the PET and MRI datasets of just a few millimeters can significantly change the calculated rCMRglc value for a particular VOI.

reasonably fast manual drawing of 3-D VOI's suitable for subsequent calculation of PET activity, uncertainties, and VOI correlations. The approach makes the implicit assumption that using MRI anatomical information is desirable while obtaining VOI's. We recognize, however, that there are other PET

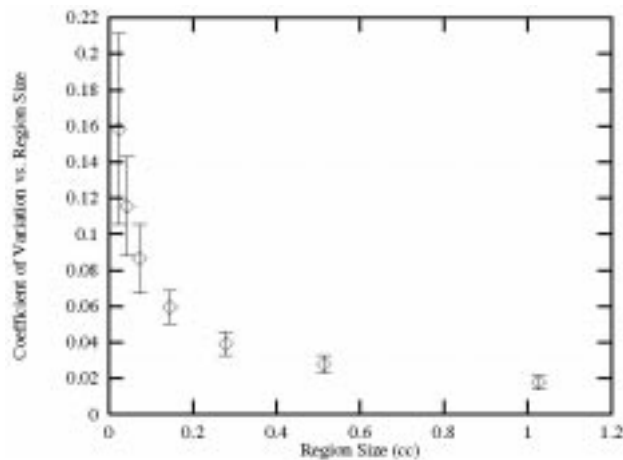


Fig. 9. PET statistical quality versus region size. Statistical uncertainty due to PET acquisition statistics is reduced with increasing region size. The coefficient of variation for regions the size of typical brain VOI is quite small.

analysis applications where use of this anatomical information may not be warranted. Region placement approaches can be classified roughly into one of two groups: anatomy based and physiology based. Anatomy-based approaches, like the one described in this paper, rely on either coregistered computed tomography (CT) or MRI data on which regions are placed, or on standardized region templates which are typically stretched or warped in some manner to best fit the current PET data [24]. Physiology-based approaches rely only on the PET data, typically drawing regions around or automatically detecting areas of peak activity via subtraction or statistical techniques on parametric images which can be derived without anatomical information [25], [26]. Nevertheless, anatomical information is often desirable and even necessary for some forms of data analysis, including dynamic studies, neuroreceptor studies, and testing specific anatomically driven neuroscience hypotheses.

An issue that exists once a structure has been confidently identified is the strategy for sampling PET data from that region. Due to the limited resolution of the PET scanner, activity seen at a given point in a PET image is the spatial convolution of activity in the neighborhood of that point. For example, in typical VOI's of cortical grey matter, there is both spill out of grey matter activity within the borders of the region as well as spill in from the activity of nearby grey and white matter. One approach to dealing with this problem is to define regions well within the anatomical borders to avoid the spillover effects on the boundaries [27], [28]. Indeed as was seen in Fig. 9, PET regions do not have to be very large to obtain a good statistical estimate of activity. For the reported FDG acquisitions, reasonable estimates of rCMRglc could be obtained from regions containing only one or two reconstructed voxels ( $0.024 \text{ cm}^3$ ). However, this strategy may not be adequate because PET activity is seldom uniform throughout an anatomical structure and, thus, sampling throughout the entire structure is usually desired to characterize it. An alternate region placement approach that deals with both the spillover effects and the uniform sampling requirement is a partial volume correction technique. These techniques define a region along the anatomical borders and model the spatial convolution

using prior knowledge of cerebro spinal fluid (CSF) and brain matter distributions. Partial volume correction approaches have been described by Meltzer and others [29]–[31]. In view of these partial volume issues, VOI's specified along true anatomical boundaries should, therefore, be thought of as a starting point for VOI analysis. For accurate quantification of tissue within these boundaries, the VOI's can be uniformly “shrunk” or eroded to avoid spillover, or corrected using prior information for partial volume effects.

This paper is concerned with how to obtain the actual 3-D boundaries of anatomical structures. One approach is to use a standard region template manipulated in some way to best fit the anatomy, another is to manually draw the regions individually on each dataset. An obvious advantage to using templates is its simplicity. Manually drawing 3-D regions can be a time consuming process. We find that 1–2 h is typically required to manually draw a set of 48 VOI's on a brain dataset. The manual technique also has the potential for inducing operator biases, though as shown in the validation section, these biases are fairly small when using anatomical landmarks from MRI data. The biases may be more troublesome if regions were drawn directly on PET data. A disadvantage to using fixed templates is that it may be difficult to suitably warp a standard region set to fit a particular patient's data. There is considerable variation in the shape and position of structures in the brain and it is still an open question whether an elastic transformation always exists to suitably transform every study into a standard space. Though a template may attempt to more completely and uniformly describe a given anatomical region set, unsuitable elastic transformations could produce unacceptable position errors for some regions. This is a problem in analysis of brain data from patients with significant anatomical variability due to cerebral atrophy, infarction, or tumors. It is for this reason that we have chosen the manual technique.

Our validation studies indicate that fairly consistent results can be expected using manual drawing techniques. For most regions, differences due to slicing orientation or operator criteria are under 5%. Slice spacing also appears to have a negligible effect as long as the chosen spacing is less than 7 mm. In practice, our clinicians typically use 3-mm slice spacing. Reported results do not include a correction for partial volume, which is beyond the scope of this paper. Most likely, the effect of slicing orientation, slice spacing, and small operator region discrepancies is to change the relative proportion of activity due to the grey matter in that VOI. Correction for partial volume would reduce this variance. Partial volume correction, however, would not correct for registration errors.

Woods [7] reported that registration accuracy of  $<2$  mm could be expected using their automatic algorithm for PET and MRI datasets, and since this is the last step in our semiautomatic registration process, we should expect comparable accuracy. The results from Section III show that mean rCMRglc differences within this range of translation are all within 5% for registration errors of 1 or 2 mm. However, the nearly linear increase in quantification error with registration offset underscores the importance of an accurate registration.

## V. CONCLUDING REMARKS

The reported technique for specifying and analyzing VOI's on PET datasets demonstrates an approach for analyzing complex 3-D datasets using common 2-D interfaces. Navigation through the dataset to find a desired anatomical structure can be greatly simplified using a registered MRI anatomical volume showing multiple simultaneous oblique sections and volume renderings of the data. Because most clinicians can readily identify specific sulci from high-quality renderings of the cortical surface, a crucial step in quickly identifying sulci in 2-D sectional data is providing a feedback mechanism between the renderings and the sectional data. Once identified, 3-D VOI's may be specified on the anatomical datasets efficiently in an X-Windows environment by drawing a stack of 2-D regions subsequently tiled together to form a VOI surface model. The voxel-independent description of the VOI's allows a quantitative analysis in the observation space of the PET scanner for characterization of both VOI radiotracer activity and statistical properties.

Results obtained from typical brain analyses indicate that the stack of regions defining a VOI may be drawn on slices oriented at the oblique slicing direction which best allows visualization of the cross section for a desired structure. A 3-mm to 7-mm slicing separation appears sufficient to capture the salient shape features of regions in the cortex. VOI's drawn using a finer slice separation produced similar quantitative results at the cost of increased manual intervention.

The registration and segmentation steps are seen to be crucial preprocessing steps in the VOI analysis. An accurate segmentation of brain from nonbrain structures is needed for high-quality surface renderings and for automated registration routines. Validation results imply that registration between PET and MRI datasets must be achieved to an accuracy better than 2 mm. Our experiences show that this level of accuracy is difficult to obtain quickly using purely manual techniques. However, by combining manual with automated registration techniques, we are able to obtain reliable registration with minimal manual burden. The manual portion of the segmentation and registration process has the additional advantage that quality control can be visually verified by a trained clinician.

## ACKNOWLEDGMENT

The authors wish to thank U. Pietrzyk and R. Woods, for providing their image registration software and the reviewers of this paper for their valuable comments.

## REFERENCES

- [1] C. C. Meltzer, R. N. Bryan, H. H. Holcomb, A. W. Kimball, H. S. Mayberg, B. Sadzot, J. P. Leal, H. N. Wagner, Jr., and J. J. Frost, "Anatomical localization for PET using MR imaging," *J. Comput. Assist. Tomogr.*, vol. 14, no. 3, pp. 418-426, 1990.
- [2] S. C. Strother, J. R. Anderson, X. Xu, J. Liow, D. C. Bonar, and D. A. Rottenberg, "Quantitative comparisons of image registration techniques based on high-resolution MRI of the brain," *J. Comput. Assist. Tomogr.*, vol. 18, no. 6, pp. 954-962, 1994.
- [3] U. Pietrzyk, K. Herholz, G. Fink, A. Jacobs, R. Mielke, I. Slansky, M. Wurker, and W. Heiss, "An interactive technique for three-dimensional image registration: Validation for PET, SPECT, MRI and CT brain studies," *J. Nucl. Med.*, vol. 35, no. 12, pp. 2011-2018, 1994.
- [4] K. Wienhard, M. Dahlbom, L. Eriksson, C. Michel, T. Bruckbauer, U. Pietrzyk, and W. Heiss, "The ECAT EXACT HR: Performance of a new high resolution positron scanner," *J. Comput. Assist. Tomogr.*, vol. 18, no. 1, pp. 110-118, 1994.
- [5] M. S. Roos, R. A. Mushlin, E. Veklerov, J. D. Port, C. Ladd, and C. G. Harrison, "An instrument control and data analysis program configured for NMR imaging," *IEEE Trans. Nucl. Sci.*, vol. 36, pp. 988-992, 1988.
- [6] C. A. Pelizzari, G. T. Y. Chen, D. R. Spelbring, R. R. Weichselbaum, and C. T. Chen, "Accurate three-dimensional registration of CT, PET, and/or MR images of the brain," *J. Comput. Assist. Tomogr.*, vol. 13, pp. 20-26, 1989.
- [7] R. P. Woods, J. C. Mazziota, and S. R. Cherry, "MR-PET registration with automated algorithm," *J. Comput. Assist. Tomogr.*, vol. 17, no. 4, pp. 536-546, 1993.
- [8] B. A. Ardekani, M. Braun, I. Kanno, and B. F. Hutton, "Automatic detection of intradural spaces in MR images," *J. Comput. Assist. Tomogr.*, vol. 18, no. 6, pp. 963-969, 1994.
- [9] U. Pietrzyk, "A rapid three-dimensional visualization technique to evaluate function in relation with anatomy of the human cortex," in *Conf. Rec. 1993 IEEE Nuclear Science Symp. and Medical Imaging Conf.*, 1993, vol. 3, pp. 1810-1812.
- [10] R. A. Peters, III, "Software for 2d and 3d mathematical morphology," Air Force Office of Scientific Research, 1991, Tech. Rep.
- [11] E. A. Hoffman, D. Gnanaprakasam, K. B. Gupta, J. D. Hoford, S. D. Kugelmass, and R. S. Kulawiec, "VIDA: An environment for multidimensional image display and analysis," *Communicat. ACM*, vol. 20, pp. 693-702, 1992.
- [12] J. Boissannat and B. Geiger, "Three-dimensional reconstruction of complex shapes based on the Delaunay triangulation," INRIA Sophia-Antipolis, Tech. Rep. 1697, 1992.
- [13] J. Wernecke, *The Inventor Mentor: Programming Object-Oriented 3D Graphics with Open Inventor, Release 2*. Reading, MA: Addison-Wesley, 1994.
- [14] S. M. Resnick, J. S. Karp, B. Turetsky, and R. E. Gur, "Comparison of anatomically-defined versus physiologically-based regional localization: Effects on PET-FDG quantitation," *J. Nucl. Med.*, vol. 34, no. 12, pp. 2201-2207, 1993.
- [15] R. E. Carson, Y. Yan, M. E. Daube-Witherspoon, N. Freedman, S. L. Bacharach, and P. Herscovitch, "An approximation formula for the variance of PET region-of-interest values," *IEEE Trans. Med. Imag.*, vol. 12, no. 2, pp. 240-250, 1993.
- [16] R. H. Huesman, "A fast new algorithm for the evaluation of regions of interest and statistical uncertainty in computed tomography," *Phys. Med. Biol.*, vol. 25, no. 5, pp. 543-552, 1984.
- [17] J. R. Votaw, "Signal-to-noise ratio in neuro activation PET studies," *IEEE Trans. Med. Imag.*, vol. 15, no. 2, pp. 197-205, 1996.
- [18] P. H. King, K. Hubner, W. Gibbs, and E. Holloway, "Noise identification and removal in positron imaging systems," *IEEE Trans. Nucl. Sci.*, vol. NS-28, no. 1, pp. 148-151, 1981.
- [19] M. Bergstrom, L. Eriksson, C. Bohm, G. Blomqvist, and J. Litton, "Correction for scattered radiation in a ring detector positron camera by integral transformation of the projections," *J. Comput. Assist. Tomogr.*, vol. 7, no. 1, pp. 42-50, 1983.
- [20] M. Defrise, D. Townsend, and A. Geissbuhler, "Implementation of three-dimensional image reconstruction for multi-ring positron tomographs," *Phys. Med. Biol.*, vol. 35, no. 10, pp. 1361-1372, 1990.
- [21] D. P. Huttenlocher, G. A. Klanderman, and W. J. Rucklidge, "Comparing images using the Hausdorff distance," *IEEE Trans. Pattern Anal. Machine. Intell.*, vol. 15, no. 9, pp. 850-863, 1993.
- [22] W. J. Jagust, J. P. Seab, R. H. Huesman, P. E. Valk, C. A. Mathis, B. R. Reed, P. G. Coxson, and T. F. Budinger, "Diminished glucose transport in Alzheimer's disease: Dynamic PET studies," *J. Cereb. Blood Flow Metab.*, vol. 11, pp. 323-330, 1991.
- [23] M. E. Phelps, S. C. Huang, E. J. Hoffman, C. Selin, L. Sokoloff, and D. E. Kuhl, "Tomographic measurement of local cerebral glucose metabolic rate in humans with (F-18)2-fluoro-2-deoxy-d-glucose: Validation of method," *Ann. Neurol.*, vol. 6, pp. 371-388, 1979.
- [24] C. Bohm, T. Greitz, R. Seitz, and L. Eriksson, "Specification and selection of regions of interest (ROI's) in a computerized brain atlas," *J. Cereb. Blood Flow Metab.*, vol. 11, pp. A64-A68, 1991.
- [25] P. T. Fox, M. A. Mintun, E. M. Reiman, and M. E. Raichle, "Enhanced detection of focal brain responses using intersubject averaging and distribution analysis of subtracted PET images," *J. Cereb. Blood Flow Metab.*, vol. 8, pp. 642-653, 1988.
- [26] K. J. Friston, C. D. Frith, P. F. Liddle, and R. Frackowiak, "Comparing functional (PET) images: The assessment of significant change," *J. Cereb. Blood Flow Metab.*, vol. 11, pp. 690-699, 1991.
- [27] E. J. Hoffman, S. Huang, and M. E. Phelps, "Quantitation in positron emission computed tomography: 1. Effect of object size," *J. Comput. Assist. Tomogr.*, vol. 3, no. 3, pp. 299-308, 1979.

- [28] J. C. Mazziotta, C. C. Pelizzari, G. T. Chen, F. L. Bookstein, and D. Valentino, "Region of interest issues: The relationship between structure and function in the brain," *J. Cereb. Blood Flow Metab.*, vol. 11, pp. A51–A56, 1991.
- [29] C. C. Meltzer, J. P. Leal, H. S. Mayberg, H. N. Wagner, Jr., and J. J. Frost, "Correction of PET data for partial volume effects in human cerebral cortex by MR imaging," *J. Comput. Assist. Tomogr.*, vol. 14, no. 4, pp. 561–570, 1990.
- [30] C. C. Meltzer, J. K. Zubieta, J. M. Links, P. Brakeman, M. J. Stumpf, and J. J. Frost, "MR-based correction of brain PET measurements for heterogeneous gray matter radioactivity distribution," *J. Cereb. Blood Flow Metab.*, vol. 16, no. 4, pp. 650–658, 1996.
- [31] H. W. Muller-Gartner, J. M. Links, J. L. Prince, R. N. Bryan, E. McVeigh, J. P. Leal, C. Davatzikos, and J. J. Frost, "Measurement of radiotracer concentration in brain gray matter using positron emission tomography: MRI-based correction for partial volume effects," *J. Cereb. Blood Flow Metab.*, vol. 12, no. 4, pp. 571–583, 1992.